CHEMISTRY
A EUROPEAN JOURNAL

DOI: 10.1002/chem.200600853

Muon Implantation of Metallocenes: Ferrocene

Upali A. Jayasooriya,*[a] Roger Grinter,[a] Penny L. Hubbard,[a] Georgina M. Aston,[a] John A. Stride,[a, d] Gareth A. Hopkins,[a] Laure Camus,[a] Ivan D. Reid,[b, e] Stephen P. Cottrell,[c] and Stephen F. J. Cox[c]

Abstract: Muon Spin Relaxation and Avoided Level Crossing (ALC) measurements of ferrocene are reported. The main features observed are five high field resonances in the ALC spectrum at about 3.26, 2.44, 2.04, 1.19 and 1.17 T, for the low-temperature phase at 18 K. The high-temperature phase at 295 K shows that only the last feature shifted down to about 0.49 T and a muon spin relaxation peak at about 0.106 T which approaches zero field when reaching the phase transition temperature of 164 K. A model involving three muoniated radicals, two with muonium addition to the cyclopentadienyl ring and the other to the metal atom, is postulated to rationalise these observations. A theoretical treatment involving spin-orbit coupling is found to be required to understand the Fe–Mu adduct, where an interesting interplay between the ferrocene ring dynamics and the spin-orbit coupling of the unpaired electron is shown to be important. The limiting temperature above which the full effect of spin-orbit interaction is observable in the μSR spectra of ferrocene was estimated to be 584 K. Correlation time for the ring rotation dynamics of the Fe–Mu radical at this temperature is 3.2 ps. Estimated electron *g* values and the changes in zero-field splittings for this temperature range are also reported.

Keywords: hydrogen · metallocenes · molecular dynamics · muons · radicals

Introduction

The positive muon, which is used as a probe in this study, is a transient particle with a lifetime of 2.2 μs. Chemically it resembles a proton with almost a ninth of the mass. On implantation into matter, the muon may exist as the positive ion, mimicking a proton or pick up an electron to form an isotopic analogue of the hydrogen atom, muonium. The muonium thus formed may add to an unsaturated centre in the molecules that compose the material to give radical species. Analogous to the proton, the muon also has a spin of one half; at the end of its life it decays to give a positron which is emitted preferentially along the spin direction at the moment of decay. Because it is possible to produce almost 100% spin polarised muon beams, detection of the direction of emission of the decay positrons allows the study of the evolution of the muon spin within the implanted sample. This provides information on the magnetic fields local to the muon site.

The study of muonium addition to organic compounds is well developed.[1] We have initiated a study of muonium addition to organometallics, mainly for the following reasons.

The dynamics of organic ligands attached to metal centres are important for catalysis. For example, "…metallocene

[a] Dr. U. A. Jayasooriya, Dr. R. Grinter, Dr. P. L. Hubbard, Dr. G. M. Aston, Dr. J. A. Stride, G. A. Hopkins, Dr. L. Camus
School of Chemical Sciences and Pharmacy
University of East Anglia
Norwich NR4 7TJ (UK)
Fax: (+44) 1603592003
E-mail: u.jayasooriya@uea.ac.uk

[b] Dr. I. D. Reid
Paul Scherrer Institut
5232 Villigen PSI (Switzerland)

[c] Dr. S. P. Cottrell, Prof. S. F. J. Cox
ISIS Facility
Rutherford Appleton Laboratory
Chilton, Didcot, Oxon OX11 0QX (UK)

[d] Dr. J. A. Stride
Present address:
School of Chemistry
Faculty of Science, University of New South Wales
Sydney, NSW 2052 (Australia)

[e] Dr. I. D. Reid
Present address:
Department of Electronic and Computer Engineering
Brunel University
Uxbridge UBH 3PH (UK)

Supporting information for this article is available on the WWW under http://www.chemeurj.org/ or from the author.

catalysts are now replacing Ziegler–Natta catalysts, making it possible to engineer the properties of polymers by design at a molecular level…".[2] The importance of metallocene ring dynamics to polymer engineering has been beautifully illustrated by Waymouth and Coates.[3] However, the ring rotation rates of these metallocenes used in the latter hypothesis were measured only very recently, but at low temperatures which are not directly relevant to the catalytic process.[4] The latter paper also provides a good description of the reasons for the difficulties in measuring these rates which are too fast for the conventional techniques. The rates of metallocene ring reorientation at the temperatures of interest happen to fall within the microsecond to picosecond time window, which bridges the accessible timescales of nuclear magnetic resonance (NMR) and quasielastic neutron scattering (QENS) with more overlap with the latter. Of the techniques applicable to this time window, Mössbauer spectroscopy is limited to very few metals. EPR, on the other hand, depends on the presence of molecules with unpaired electrons, and some of these may be EPR-silent. The lower end of this time window could be accessed using deuterium NMR, and the range could be extended by an order of magnitude using fully deuteriated samples. μSR has the potential to be a versatile technique for this time window, being applicable to all unsaturated systems. It is the open shell radical species that is studied in μSR, not the closed shell parent. However, as illustrated in this study, it appears that there are situations, such as the occupation of a nonbonding orbital, where the extra electron does not significantly change some of the important dynamics of the molecule.

It is not possible to use NMR to study the dynamics of molecules or groups when next to a conducting material such as in polymer composites with graphite or metals, or molecules on metal surfaces in heterogeneous catalysis. QENS experiments may be used for this purpose but requires samples with large surface areas in order to have sufficient material on the surface, which is not often possible. With the advent of the "slow muon beams", which are currently being developed at some muon facilities, it is already possible to study thin films; surfaces may be accessible in the future. Therefore the development of μSR as a method to probe the dynamics of species on metal surfaces is likely to produce uniquely important information on heterogeneous catalysis. A study in the literature of relevance to this is the investigation of the dynamics of benzene molecules on finely divided silica by Reid et al.[5] Another study of relevance to catalysis is the μSR assisted deduction of the reason for increased reactivity of ferrocene when encapsulated within a zeolite.[6]

Muon implantation studies are in essence a method to make novel organometallic hydride analogues, using the accepted analogy of muonium as a lighter isotope of hydrogen,[1] and studying their properties in a rather convenient way. If found to have interesting and useful properties, the hydrides corresponding to these adducts might then be prepared by suitably designed syntheses. Such adducts for example, are postulated to be responsible for the termination of catalytic activity in the metallocene catalysis of polypropylene formation.[7]

A number of theoretical treatments of protonation of ferrocene can be found in the literature,[8] but none on the addition of hydrogen atoms to metallocenes. Macrae[9] has recently attempted to calculate the addition of muonium to ferrocene. He reported on the energy minimum structures for three likely adducts, one to the metal and two to the cyclopentadienyl ring, Figure 1. However, the methods used (including DFT) does not provide a satisfactory way of dealing with the spin-orbit coupling that is clearly expected to be significant with transition metals.[11] Therefore we have taken a well proven approach, similar to that of Ammeter and Swalen[12] to deal with this problem as described later in this paper.

Herein we report a detailed study of the addition of muonium, the lightest isotope of hydrogen, to ferrocene, an assignment of the resulting spectral features and an evaluation of the corresponding hyperfine parameters.[10] From this example it is clear that muoniated systems present very interesting theoretical problems that are complex but solvable, thus opening the way for the study of hydrogen atom additions to metallocenes using the elegant method of muon implantation.

Results and Discussion

The field of organometallic chemistry was transformed in 1952[13] by the discovery of the "sandwich" structure of what has become the most famous member of this family of compounds, dicyclopentadienyl iron or ferrocene. A wealth of knowledge now exists on its structure and dynamics, including NMR spectroscopy[14] and QENS[15] studies. For that reason ferrocene was chosen for this investigation to determine the suitability of μSR for the study of organometallic compounds. Ferrocene undergoes a phase transition at 163.9 K.[16] During the present series of studies this phase change was observed to show substantial hysteresis.[17] X-ray crystal structure determinations at 295 and 173 K[18] show the high temperature phase (HT) to be monoclinic, space group $P2_1/a$ with $Z=2$. This phase is also found to possess rotational disorder.

Of relevance to this investigation is the present understanding of the molecular orbital energy levels of ferrocene, particularly the frontier orbitals. Many calculations of the molecular orbitals of ferrocene[19,20] are to be found in the literature. There is a general consensus on the energy ordering of the molecular orbitals up to the HOMO. However, the precise ordering of the LUMO and higher levels is still uncertain; recent work having assigned the antibonding e_{1g} (xz,yz pair) as the LUMO,[18,19] closely followed by the nonbonding e_{2u} pair localised within the cyclopentadienyl rings.

The reason for the difficulty in the assignment of the LUMO orbital becomes clear when one considers the photoelectron spectroscopic work on ferrocene by Evans et al.[21] Particularly the plot of the ioinisation energies of

the isoelectronic metallocenes $[(C_6H_6)_2Cr]$, $[(C_6H_6)Mn(C_5H_5)]$ and $[(C_5H_5)_2Fe]$ (see Figure 6 in ref. [20]). There is a clear cross over in energy of the two candidate states for the HOMO, $^2A_{1g}$ and $^2E_{2g}$, close to the position of the element Fe when moving across the 1st transition metal series. Further the change in ionisation energies of the configuration $^2A_{1g}$ closely resembles those of the d orbitals of the isolated metal atoms consistent with the nonbonding nature of the a'_{1g} ($3d_z^2$) orbital.[22] It is therefore reasonable to expect a similar cross over in energy between the candidates for the LUMO, that is, the antibonding e_{1g} (xz,yz) which has an admixture of metal and ligand character, and the nonbonding e_{2u} pair confined to the cyclopentadienyl ring. Discussion of the μSR data to follow is based on this picture of the bonding in ferrocene as the starting point.

Muon spin relaxation and ALC measurements on ferrocene were made spanning the temperature range from about 300 to 18 K; the features observed are summarised in Table 1.

Table 1. Summary of experimental data for muon–$FeCp_2$ adducts.[a]

Metal adduct Phase	T/K	Observed resonances/mT Time differential measurements (Figure 10)	Time integral measurements (Figure 7)
HT	295	106.3	490.6
HT	250	64.3	–
HT	200	37.4	659.4
HT	180	27.6	699.1
phase transition	164[b]		
LT	100	–	838.1
LT	60	–	897.7
LT	18	–	1165.8
ring adducts		Observed bands/mT	
LT (μ-*endo*)	18	–	1190; 2040
LT (μ-*exo*)	18	–	2440; 3260

[a] Note that 1) The field-dependence of muon spin relaxation data indicate that there are two or more different radical species present in the sample following muon implantation. 2) The assignments of the various experimental features to particular radical species are justified in the theoretical section. 3) Peak positions were determined by using derivative spectra. [b] Phase transition temperature as reported by Edwards et al.[16] However, the present study showed that fast heating and cooling shows this transition to show significant hysteresis.

The observation of avoided level crossing resonances is dependent on a static or time averaged interaction which mixes the crossing levels, whereas the muon spin relaxation in these systems is caused by transitions induced by fluctuations of the muon's magnetic environment due, for example, to librations of groups of atoms within the molecule or vibrations and rotations of the molecule as a whole.

There are three possible adducts of muonium[9,10] to ferrocene, resulting in the radicals shown in Figure 1. All three radical species are needed to rationalise the results presented in this paper (see below). Data are first presented with assignments to the appropriate radicals, and this is followed by the theoretical treatments that justify these assignments.

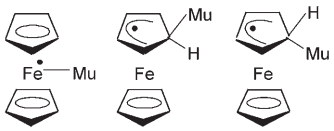

Figure 1. Metal–Mu and ring–Mu adducts of muoniated ferrocene.

The field dependence of the muon spin relaxation rate for muons implanted into polycrystalline ferrocene was measured from 2.5–400 mT at 300 K on the EMU spectrometer at the ISIS-RAL facility. At least two exponential functions were needed for good fits to the data (see Figure 2), in addition to the non-relaxing diamagnetic background. At low fields, the fast-relaxing component appears to become too fast to be measured at ISIS-RAL while the slow-relaxing component was easily measured due to the low background of the pulsed source. Although the coupled muon–electron spin states provide a multilevel system, the manner in which LF-μSR picks out the muon polarization via the asymmetry in the muon decay should lead to a relaxation curve which is effectively a single exponential.[23] The observation of two exponential components therefore implies the participation of at least two distinct chemical species.

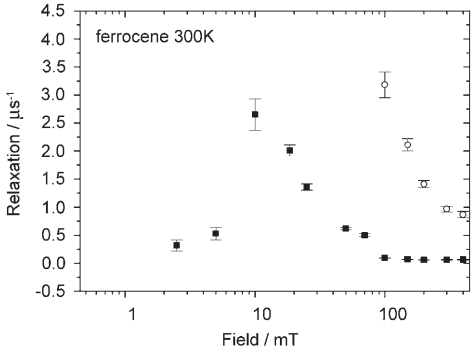

Figure 2. Field dependence of slow and fast relaxing components at 300 K.

The plot of initial asymmetry against the applied field for the slow-relaxing component showed a repolarization field of about 20 mT, a value close to that observed for muoniated benzene,[1,23] which would suggest assignment to a cyclopentadienyl ring adduct. At an applied field of 200 mT the temperature dependence of the LF-μSR relaxation rate of this slower relaxing component has a maximum around 225 K. This was shown[17] to be due to an Arrhenius process with an activation energy of about 5.39 kJ mol^{-1} and an attempt frequency of 1.03×10^{12} s^{-1}. This process is assigned by comparison with NMR[14] and QENS[15] data to the cyclopentadienyl ring rotation of ferrocene in the room temperature phase (see Table 2).

These measurements were repeated during the present study (Figure 3) also investigating the temperature dependence of the LF-μSR relaxation rate of the fast-relaxing com-

Table 2. Activation energies (E_a) and attempt frequencies (A) for ferrocene ring rotation as estimated by all the methods reported in the literature compared with those from the present investigation.

Method	Phase	E_a [kJ mol^{-1}]	[s^{-1}]	Ref.
NMR	solid $<$ 164 K	5.4(0.5)	2.2×10^{12}	[14]
NMR[a]	solid 150–300 K	5.3(0.5)		[14]
QENS	solid $>$164 K	4.4(0.5)	0.8×10^{12}	[15]
μSR[b]	solid ca. 300 K	5.39	1.03×10^{12}	[17]
μSR				
	solid ca. 300 K	5.85 (0.40)	$1.13\ (0.40)\times10^{12}$	[c]
		3.41(0.42)	$6.3\ (1.7)\times10^{11}$	[d]

[a] Results for the monoclinic phase as used for the μSR studies. [b] Slow-relaxing component. [c] Slow relaxing component in the present investigation. [d] Fast relaxing component in the present investigation.

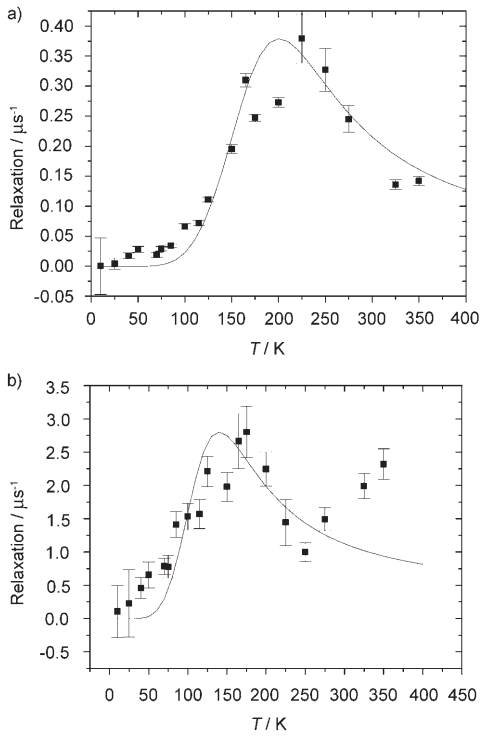

Figure 3. Temperature dependence of the two relaxing components at an applied field of 200 mT. a) Fast relaxing Fe–Mu radical. b) slow relaxing C–Mu radicals. The lines are the expected variations from the estimated Arrhenius parameters from Figure 4.

ponent at an applied field of 200 mT. The latter showed a maximum around 175 K with the relaxation dropping to a minimum around 250 K and then steadily rising at higher temperatures. A treatment of the relaxation peak at 175 K, similar to that reported for the slow-relaxing component again showed an Arrhenius process, but with an activation energy of about 3.41(0.42) kJ mol^{-1} and an attempt frequency of 6.3 $(1.7)\times10^{11}$ s^{-1} (see Figure 4a). Interestingly the value for the activation energy in this case is almost half that reported for the slow relaxing component.[17] The steady rise in relaxation beyond 250 K is due to the influence of the other more energetic dynamic processes of the

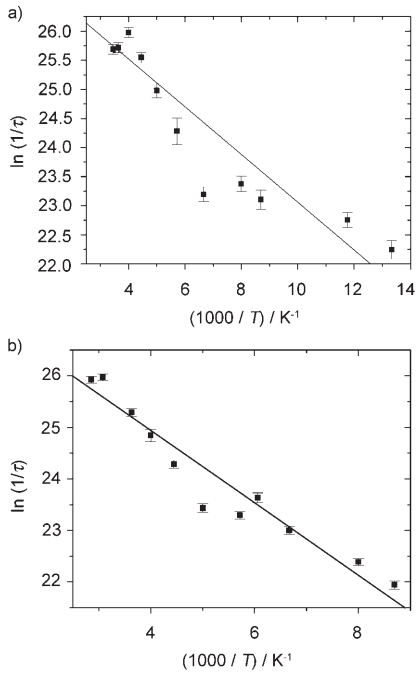

Figure 4. Arrhenius plots of the two relaxing components a) fast; the linear fit is; $[\ln(1/\tau)=27.17(\pm0.33)-0.41(\pm0.05).(1000/T)]$. b) Slow; the linear fit is; $[\ln(1/\tau)=27.76(\pm0.33)-0.70(\pm0.06).(1000/T)]$. τ is the correlation time as estimated from the muon experiment.

molecule. Similar shaped curves are reported for other spin relaxation measurements, for an example see the work done by Nakagawa et al.[25] with EPR of chromium(V) compounds. Figure 4b shows the repeated analysis of the slow relaxing component that gives the values of about 5.85-(0.40) kJ mol^{-1} and $1.13(0.40)\times10^{12}$ s^{-1} for the activation energy and the attempt frequency, respectively, in good agreement with the original report.[17] Note that the phase transition assigned to a temperature of about 164 K is found to show a large hysteresis thus making it possible to obtain measurements of the high temperature phase to much lower temperatures.

The radical species, which results from the addition of muonium to the closed-shell compound, has been investigated by μSR. In studies of molecular, "whole body", dynamics where the muon appears to be an almost passive observer, it is the very light mass of the muon which allows the observation of properties; these are almost identical to those of the parent molecule. There are a number of such studies of organic systems.[1] μSR studies of the dynamics of fullerenes C_{60} and C_{70} are particularly interesting examples of such whole body motions where the change in the moment of inertia due to the added muonium is negligible.[26] However, the use of μSR to study intramolecular dynamics presents at least two distinct scenarios.

1) The radical electron may have a *passive* role with regards to the dynamic process that is investigated. This is based on the fact that this electron will occupy an orbital such as a non-bonding molecular orbital, which plays no role

in bonding with respect to the bonds directly involved in this dynamic process.

or

2) The radical electron may have an *active* role with regards to the dynamic process that is investigated. This may be achieved by this electron occupying either a bonding or an anti-bonding molecular orbital with respect to the bonds directly involved in this dynamic process.

In looking for the assignments for the dynamic processes measured in these μSR experiments, it is important to note that the cyclopentadienyl ring rotation is the low energy dynamic process which has the largest amplitudes of motion.[27] Therefore the relaxation maxima observed for both the slow and fast relaxing components are assigned to this same dynamic process but in at least two different radical species.

A comparison with the literature reports on this dynamic process in the closed-shell compound shows that these two radicals are examples of the two types of radicals mentioned above, where either a passive or an active role is played by the radical electron.

The hyperfine interaction estimated by the muon repolarisation data justifies the assignment of the slow relaxing component to a ring adduct (Figure 1).[17] We assign an approximate molecular orbital energy level diagram for this radical to be one with the radical electron occupying the non-bonding e_{2u} pair of orbitals localised within the cyclopentadienyl rings, thus playing a passive role with respect to the dynamic process that is monitored, Figure 5. This then explains the close agreement between the activation parameters measured with μSR with those of NMR and QENS. In contrast the fast relaxing radical with only about half the activation energy for this dynamic process is an example of the radical electron playing an active role in reducing the bonding between the cyclopentadienyl rings and the iron atom. An approximate molecular orbital energy level diagram for this radical would therefore be one with the radical electron occupying the anti-bonding e_{1g} (xz,yz) orbitals (Figure 6). Note that the unpaired electron in the latter case is also associated with the heavy atom, iron, thus making spin-orbit coupling effects important for this radical. It is now possible to show that these assignments do provide an explanation of the rest of the μSR data. The near degeneracy of these two orbitals in ferrocene[21] makes these assignments reasonable.

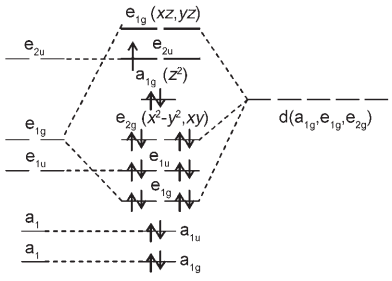

Figure 5. Postulated molecular orbital energy-level diagram for ring C–muon adduct radicals.

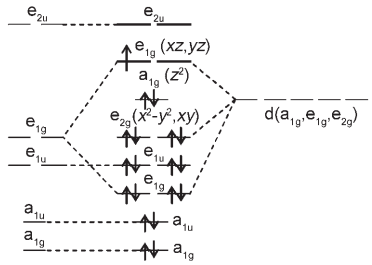

Figure 6. Postulated molecular orbital energy-level diagram for Fe–muon adduct radical.

Figure 7 shows the results of a high longitudinal-field-time integral measurement, carried out at PSI where several ALC or "avoided level crossing" resonances were observed.

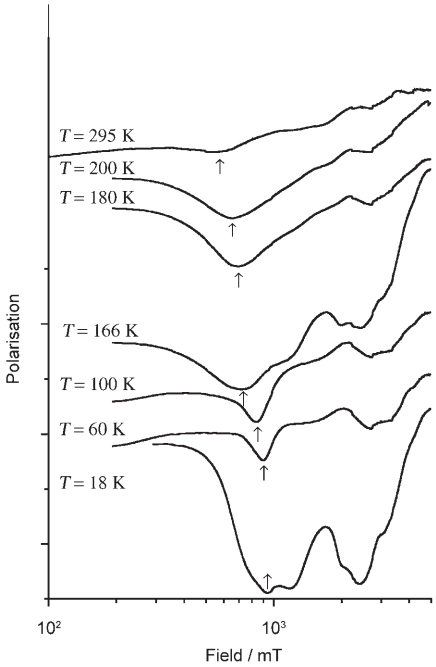

Figure 7. High-field time integral spectra (ALC) at different temperatures. The errors in polarisation measurements are within the width of the trace. The lines are guide to the eye.

A polycrystalline sample was used, and five broad features were observed, most clearly at 18 K, the lowest temperature of the experiment. The temperature dependence segregates these peaks into two sets. The high field peaks at about 3.26, 2.44, 2.04 and 1.19 T all show exceptional broadening with increase of temperature, accompanied by a slight shift towards higher fields. These resonances are broadened beyond recognition well before approaching the phase transition temperature. In marked contrast, the lowest field peak at about 1.1658 T (at 18 K) broadens less and shifts significantly to lower fields with rise in temperature. These field shifts with temperature are shown in Figure 8.

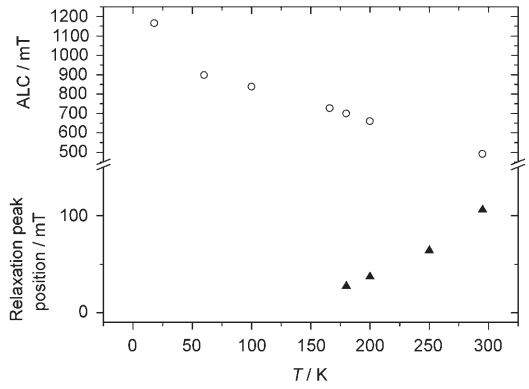

Figure 8. Temperature dependence of the high field ALC resonance (○) and the low field relaxation (▲) peak position of the Fe–Mu radical.

The comparison of the LF-time integral measurements of a ferrocene sample with that where all hydrogen atoms are replaced by deuterium is shown in Figure 9. This compound, $Fe(C_5D_5)_2$, has the strong feature at about 1.1658 T remaining almost unchanged by deuterium substitution, while the higher field polarisation losses appear significantly reduced in intensity.

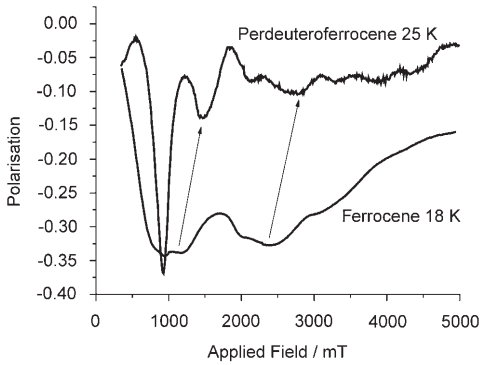

Figure 9. A comparison between the high-field time integral spectra (ALC) of ferrocene and perdeuteroferrocene.

This is what one would expect with the H/D replacement, when only the $\Delta M = 1$ transitions are expected to remain, but shifted slightly up field, to about 1.5 T and about 2.5 T, due to the replacement of H by D in the methylene position.[28,29] The metal–Mu radical where there are no protons in a methylene position should have the $\Delta M = 1$ resonance almost unchanged with H/D substitution.

In another experiment, the field dependence of the muon spin relaxation rate in a longitudinal field was measured at the PSI, where the continuous muon source makes it possible to measure shorter relaxation times than with a pulsed source, thus making faster relaxation rates accessible. However, continuous sources tend to have higher background levels. This resulted in an adequate modelling of the relaxations by a single exponential corresponding to the faster relaxing component in the ISIS data. The relaxation data for temperatures from about 300 to 100 K, where one finds the high temperature phase, are shown in Figure 10. For this fast relaxing radical a temperature-dependent relaxation peak which shifts from about 110 mT at 295 K to almost zero field at the phase transition temperature is observed (see Figure 8).

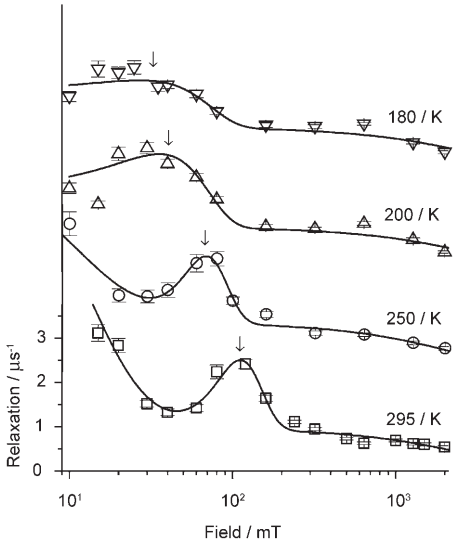

Figure 10. Muon spin relaxation dependence on field at different temperatures of the fast relaxing radical. The lines are guide to the eye.

All data on the high temperature phase of ferrocene, which were collected at the continuous muon source at the PSI and including both time differential and time integral measurements, show detectable broad (solid state) features assignable to the muonium-to-metal adduct radical that is postulated. Their resonance fields are plotted with temperature in Figure 8. We now present a theoretical treatment of this adduct that explains these variations and justifies the assignments and interpretations of all observations that were made up to now.

Muonium–iron radical of ferrocene: To our knowledge the present measurements constitute the first observation of this type of muonium adduct, where a muon is bonded directly to a heavy atom such as iron. For the interpretation of the results we need to consider a plethora of interactions such as spin-orbit coupling, crystal-field splitting and quenching of orbital angular momentum. Accordingly, a number of approximations have been made in order to make the problem tractable and facilitate the analysis of the data. In particular, we have assumed that:

1) A molecular orbital description[19–21] of metallocenes is applicable and the electronic configuration of the muonium–metal adduct is similar to that of "cobaltocene" in which the unpaired electron occupies one of a pair of degenerate orbitals designated e_{1g} in D_{5d} symmetry

(Figure 6). This pair of orbitals is derived from the atomic 3d orbitals which have m_l values of ± 1 and may be expected to retain their orbital angular momentum under conditions of high axial symmetry.

2) The above electronic orbital angular momentum may be partially quenched by bonding, and this is allowed for in the present treatment by the introduction of a parameter γ; $0.0 \leq \gamma \leq 1.0$, where $\gamma = 1.0$ represents the unquenched situation.
3) The degeneracy of the 3d orbitals having $m_l = \pm 1$ may be lifted by forces in the solid state or by the formation of the muonium adduct. Following Ammeter and Swalen,[12] we allow for this fact by introducing off-diagonal matrix elements $\pm iV$ (where $i = \sqrt{-1}$) between states having $m_l = +1$ and those with $m_l = -1$ into the energy matrix. V is a crystal or ligand field parameter.
4) Significant spin-orbit coupling (spin-orbit coupling constant ζ) must also be assumed. The effects of the parameters V, γ and ζ upon the electronic structure of the molecule have been discussed by Ammeter and Swalen,[12] in their detailed study of the electron paramagnetic resonance of cobaltocene. In this work we also observe a subtle interplay between them.
5) The system may be adequately described by a basis of eight microstates ($|m_l(e), m_s(e), m_s(\mu)\rangle$) consisting of two possible values of the z component of the electronic orbital angular momentum, two possible spin orientations each of the unpaired electron and the muon. For a complete treatment many more states would be required since spin-orbit coupling connects microstates with $m_l = \pm 1$ with others having $m_l = 0$ and ± 2.
6) The magnetic interactions can be generated (in frequency units) using the Hamiltonian:

$$\hat{H} = \gamma\varsigma \hat{\mathbf{l}} \cdot \hat{\mathbf{S}} + A_\mu \hat{\mathbf{I}} \cdot \hat{\mathbf{S}} + \mathrm{B}[(^1/_2 \gamma \hat{l}_z + \hat{S}_z)\nu_e - \hat{I}_{\mu z}\nu_\mu]$$

where, $\hat{\mathbf{l}}$, $\hat{l}_z$, $\hat{\mathbf{S}}$, $\hat{S}_z$, $\hat{\mathbf{I}}_\mu$ and $\hat{I}_{\mu z}$ are the operators for the orbital and spin angular momenta of the unpaired electron and the muon spin respectively; each followed by its z component. A_μ is the muon coupling constant and V, γ and ζ have been defined above. The Hamiltonian has been formulated so that all Larmor frequencies are positive, namely: $\nu_e = +8.0\,\mathrm{GHz\,T^{-1}}$, $\nu_\mu = +135.5\,\mathrm{MHz\,T^{-1}}$ and $\nu_p = +42.6\,\mathrm{MHz\,T^{-1}}$. ν_p is the Larmor frequency of the proton which we introduce here for use below. The matrix of $\hat{H}$ for the eight basis microstates, $|m_l(e), m_s(e), m_s(\mu)\rangle$, blocks out into two 2×2 and one 4×4 matrices. When $B = 0$ these matrices can be diagonalised algebraically giving the following eight eigenvalues. These matrices and the detailed calculations are shown in Appendix SI, in the Supporting Information.

From the two 2×2 matrices:

$$E = (A_\mu/4) \pm \sqrt{\{\gamma\zeta/2)^2 + V^2\}}$$

two of each, four eigenvalues in total.

From the 4×4 matrix:

$$E = -(A_\mu/4) \pm \sqrt{\{\gamma\zeta/2)^2 + (A_\mu/2 \pm V)^2\}}$$

all four sign combinations.

In order to visualise the way in which the energy changes with spin-orbit coupling and crystal field, it is easier to first consider the two extreme cases of $\gamma\zeta = 0$ and $V = 0$.

At $\gamma\zeta = 0$ we have two sets of energy levels with their energetic centres of gravity separated by $2V$. Each set comprises a threefold degenerate level at $V + 0.25A_\mu$ (or $-V + 0.25A_\mu$) and a single level at $V - 0.75A_\mu$ (or $-V - 0.75A_\mu$).

At $V = 0$, there are four degenerate pairs of energy levels. An upper set of two pairs at $0.25A_\mu + 0.5\gamma\zeta$ and $-0.25A_\mu + 0.5\sqrt{\{(\gamma\zeta)^2 + A_\mu{}^2\}}$ and a lower set of two pairs at $0.25A_\mu - 0.5\gamma\zeta$ and $-0.25A_\mu - 0.5\sqrt{\{(\gamma\zeta)^2 + A_\mu{}^2\}}$.

A diagram such as depicted in Figure 11 may be drawn in terms of the parameter $V/\gamma\zeta$ in order to correlate these two extremes. The lower four energy levels only are plotted, the

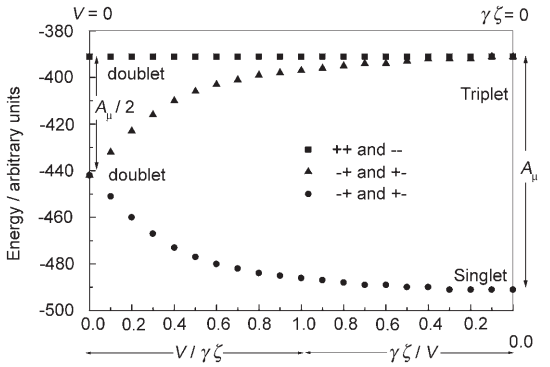

Figure 11. Energy level dependence on the interplay between spin-orbit coupling and crystal field effects at zero applied field. ++, −−, +− and −+ represent the spin functions of the electron and the muon in the wave functions.

higher four show the same behaviour. Therefore Figure 11 illustrates the predicted variation of zero-field splitting depending on the interplay between the spin-orbit coupling and the crystal field. A vertical line on the diagram is the starting position from which the levels diverge/converge when an increasing external magnetic field is applied (see Figure 12), which is predicted to result in two level crossings at fields of B_a and B_b. It is to be noted that the level of approximation used in this analysis results in these being true level crossings. However, the use of a more realistic Hamiltonian or coupling of the states involved via an energetically distant energy level will result in the lifting of the degeneracy at these crossings as observed for many other systems.[1] The assignment of these level crossings to the experimentally observed ALCs is therefore based on this realistic expectation.

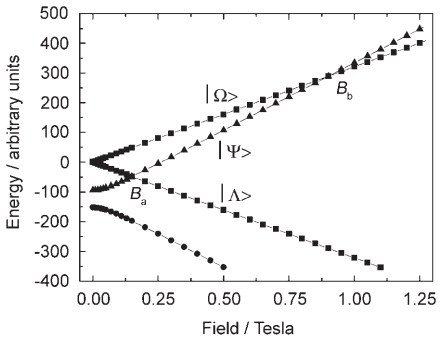

Figure 12. Theoretical level crossings for metal–μ adduct in ferrocene.

The results depicted in Figures 11 and 12 predict the crossings B_a and B_b to change with temperature due to the variation of the quantity $V/\gamma\zeta$. Such a change is experimentally observed for the two unique resonances for the high temperature phase as shown in Figures 7 and 9 and is illustrated in Figure 8.

Though there may be some uncertainty as to the value of V (see below), ζ for the iron atom is certainly in the order of 10^7 MHz[11] and is the order of energy separation to be expected between the two sets of four energy levels at the $V=0$ extreme. Thus, the model presented here provides a reasonable explanation for the two resonances, B_a and B_b ($B_a < B_b$; see also Table 1), in terms of the lower group of four energy levels; these resonances are therefore assigned to the metal–Mu radical.

The problem is made rather complicated by the presence of the parameters V, ζ and γ and our inability to diagonalise the matrices algebraically when $B \neq 0$. However, explicit diagonalisation of matrices generated with a range of parameters shows that the dependence of the lower four levels upon magnetic field is effectively linear above 250 mT (Figure 12) and that the simple relationship $A_\mu = 2\ B_b \nu_\mu$, as explained in Appendix II (Supporting Information), gives values of A_μ in good agreement with the results of full matrix diagonalisation with $\gamma = 1.0$. If the value of A_μ is fixed in this way for a particular B_b then pairs of values of γ and V can be determined by full diagonalisation which gives an ALC at B_a and a new predicted B_b which is found to differ by less than 1% from the experimental value used to determine A_μ. Agreement was further improved by refining the value of A_μ to reduce the rms difference between the experimental and calculated ALC resonance fields to a minimum (see Table 3).

Table 3. Calculated values of metal-adduct parameters with γ fixed and $\zeta = 2.6\times10^7$ MHz.

T/K		295	250	200	180
B_a [mT]	exptl	106	64	37	28
B_b [mT]	exptl	491	571*	659	699
γ	calcd	1.0	1.0	1.0	1.0
$V\times10^5$ [MHz]	calcd	27.5	38.0	53.1	63.2
A_μ [MHz]	calcd	134	156	180	191
B_a [mT]	calcd	106	64	37	28
B_b [mT]	calcd	489	569	657	697
rel. intensities B_b/B_a	calcd	6.0	4.1	3.0	2.6
$V/\gamma\xi$	calcd	0.11	0.15	0.20	0.24

[*] Estimated by interpolation.

The results in Table 3 only include entries for $\gamma = 1.0$ since it was found that the ALC values at 295 K cannot be reproduced with a γ value lower that 0.98 while the data at 200 and 180 K are incompatible with values of γ below ≈ 0.9. For the data at 180 K, a range of seven paired γ and V values can be determined for $1.0 \geq \gamma \geq 0.88$. It is found that V and γ are linearly related according to the following equation:

$$V \times 10^{-5} = (434.7\gamma - 369.0)\ \text{MHz}$$

with a correlation coefficient of 0.978. There is a similar linear relationship between V and γ for other temperatures, though the range of γ values is much smaller and the gradient becomes somewhat steeper as the temperature rises. The linear relationship between V and γ confirms the intuitive feeling that both parameters reflect essentially the same phenomenon in slightly different ways. Any loss of the degeneracy, that is, an increase of V, of the $m_l = \pm 1$ levels will decrease the orbital angular momentum which can be represented by a decrease in the value of γ.

At the present state of refinement of the model it therefore appears possible to view the changes in the positions of the ALC's as being the result of changes of V and/or γ. Studies of other metallocenes which have been performed in an attempt to clarify the position are in progress. Muon spectroscopy may therefore offer a novel way of investigating the quenching of orbital angular momentum.

The analysis in this paper provides clear assignments of the state of the system to positions on the horizontal axis of Figure 11 for the four temperatures at which both B_a and B_b measurements were made. Our model also allows us to make tentative predictions concerning the relative ability of each ALC to bring about a muon spin-flip relaxation, that is the possible mixing of the states via the above-mentioned mechanisms or the intensity of the ALC signals (see Appendix SII in the Supporting Information for further discussion). Electron g factors for this system at different temperatures are also estimated as illustrated in Appendix SIII (see Supporting Information). It is worth exploring the possibility of finding a parameter based on the model of spin-orbit coupling developed here to explain the μSR data as a measure of spin-orbit coupling in different metallocenes. A plot of the estimated values of the ratio $V/\gamma\xi$ (see Table 3) against the natural logarithm of the correlation times for the ring dynamics of the Fe–Mu radical—as estimated based on the Arrhenius plot given in Figure 4a—is shown in Figure 13a. There is a good linear correlation between these quantities, giving a value of about 3.2 ± 0.1 ps for τ at zero crystal field. It is interesting to compare this value with τ_8 of about 1.6 ps obtained with the Arrhenius plot from the spin lattice relaxation data alone (see Figure 4) and reported as 2.2(7) ps for

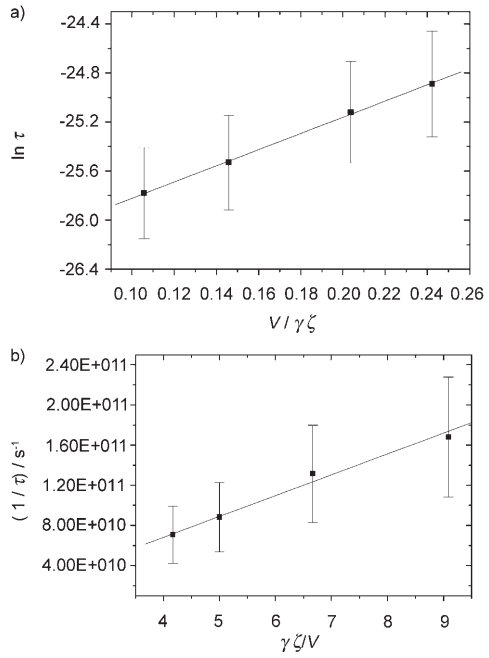

Figure 13. Relationship between the correlation times obtained from the spin-lattice relaxation data and the ratio between the crystal field splitting parameter V and the spin-orbit coupling constant ζ. Fits: a) $\ln \tau = 6.61(0.14)\ (V/\gamma\zeta - 26.48(0.03)$and b) $1/\tau = 2.07(0.17)\times 10^{10}\ (\gamma\zeta/V) - 1.47(0.95)\times 10^{10}$.

the Fe–Mu radical by Kaiser et al.[32] using a limited data set. Now if one were to use the correlation time of 3.2 ps, it is possible to estimate the temperature at which this value is reached for this particular radical using the Arrhenius plot given in Figure 4. This value of about 584 K corresponds to the left-hand end of Figure 11 where one would observe the maximum manifestation of the spin-orbit interaction as a zero-field splitting.

Figure 13b shows the relationship between the correlation times and the quantity $\gamma\zeta/V$, where the simplest linear relationship is between $1/\tau$ and $\gamma\zeta/V$. Interestingly, this plot gives a negative intercept on the $1/\tau$ axis, with the intercept on the $\gamma\zeta/V$ axis at 0.71 ± 0.46. Therefore a vertical line through this value of $\gamma\zeta/V$ in Figure 11 gives the zero-field splittings to be expected at the extreme case of static cyclopentadienyl rings. This is reasonable as an orbital contribution would be expected to be present even when the cyclopentadienyl rings are static. Since the zero-field splitting for ferrocene is predicted to have reached a maximum at 584 K, this may be used to characterise ferrocene and thus be used as a μSR measure of the interplay between the intramolecular dynamics and spin-orbit coupling in the Fe–Mu radical, and would be a useful parameter for comparison between different metallocenes.

As a final comment upon our interpretation of the muonium–metal adduct spectra we emphasise again that our approach contains several parameters, and the values that these should take in this particular model, are difficult to determine by alternative methods. Indeed, the model itself must, at this stage, be regarded as tentative and in need of further applications to other organometallic–muonium adducts to test its viability.

Muonium addition to the cyclopentadienyl ring of ferrocene: To interpret the ALC's of the ring adducts we have followed the approach of Roduner and his co-workers[5,30] closely. The notation for the proton is analogous to that used for the muon μ being replaced by p so that we formulate the Hamiltonian as:

$$\hat{H} = A_\mu \hat{\mathbf{I}} \cdot \hat{\mathbf{S}} + A_p \hat{\mathbf{I}}_p \cdot \hat{\mathbf{S}} + B[\hat{S}_z \nu_e - \hat{I}_{pz} \nu_p - \hat{I}_{\mu z} \nu_\mu]$$

As shown by Reid et al.,[5] very good estimates of the fields at which the high-field ALCs occur may be obtained as follows:

For the proton-muon spin flip–flop where $\Delta M = 0$

$$B_0 = |\frac{A_\mu - A_p}{2(\nu_\mu - \nu_p)}|$$

and for the muon spin flip where $\Delta M = 1$

$$B_1 = |\frac{A\mu}{2\nu_\mu}|$$

Though these equations may be refined,[29] we find that the resulting values for B_0 and B_1 are in good agreement with full matrix diagonalisation. The values of A_μ and A_p found using the above equations provide the starting point for our attempts to interpret the four peaks in the region between 1 and 4 T, where the ALC's of the ring adduct are expected. The presence of four rather than two peaks in the high-field region suggests the presence of two muonium–cyclopentadienyl ring-adduct radicals. We believe that the two radicals are distinguished by the relative positions of the muon and proton bound to the, approximately tetrahedral, carbon atom carrying the former. We call the adduct with the muon on the same side of the ring as the iron atom the *endo*-muon species and that with the proton closer to the iron atom the *exo*-muon (see Figure 1). This interpretation receives strong support from recent studies of the benzene–muon radical in NaY zeolites by Fleming et al.[30] who found four ALC's between 1.5 and 3 T. They attributed the two bands at lower fields, for which they found $A_\mu = 430$ and $A_p = 70$ MHz, to an adduct with the muon on the same side of the benzene ring as the cation and the two bands at higher fields ($A_\mu = 606$ and $A_p = 108$ MHz) to an adduct with the muon on the other side of the ring, remote from the cation. Our task therefore is to assign our experimental features to the B_0 and B_1 ALC's of the two possible ring adducts.

Examination of all possible assignments leads to the conclusion that for one species $B_0 = 2.04$ and $B_1 = 1.19$ T yield $A_\mu = 322$ and $A_p = -57$ MHz, while for the second species

$B_0 = 3.26$ and $B_1 = 2.44$ T yield $A_\mu = 661$ and $A_p = 55$ MHz. Where we have also assumed, in the light of earlier results,[31] that A_μ is always positive in systems of this type (see Table 4).

Table 4. Comparison of the experimental values of the ALCs with those calculated from estimates of A_μ and A_p for the ring adducts.

A_p [MHz]	A_μ [MHz]	B_1 [T]	B_0 [T]
		muon-*endo*	
		1.19 (exptl)	2.04 (exptl)
−57	324	1.19	2.04
−25	335	1.230	1.93
		muon-*exo*	
		2.44 (exptl)	3.26 (exptl)
57	665	2.44	3.26
19	645	2.37	3.35

A comparison of the features observed for the fully H and fully D species (Figure 8) shows the retention of the features assigned to the $\Delta M = 1$ transitions albeit with some shifts thus confirming these assignments. Shifts in the field positions of about 20 mT with deuteriation are as expected.[28,29]

Conclusions

Muon spin relaxation and avoided level crossing experiments have been made on polycrystalline samples of ferrocene both in its high temperature and low temperature phases. Also reported are the measurements of a fully deuterium substituted sample. The observations have been rationalised by assuming the formation of all three radical species, two muonium adducts to the cyclopentadienyl ring and one to the metal. The ring adduct data are interpreted with the theoretical treatments already in the literature for addition to organic ring systems. Molecular orbital energy level diagrams for these radicals have been postulated and theoretical models, including spin-orbit coupling and crystal field effects, developed in order to account especially for the unusual temperature variations of the resonances due to the metal–Mu adduct, a novel radical species. It is found that when the value of the quenching of the orbital motion γ is assumed to be 1, a value justified in the discussion, the ratio of crystal field to spin orbit coupling $V/\gamma\xi$ (Table 3) is unique for a particular set of the level crossings B_a and B_b, and therefore is fixed for a given temperature. This therefore uniquely defines the state of the zero-field splittings for this system at a particular temperature; the positions are indicated in Table 3. This Table also gives the theoretically estimated ratio of the intensities of the polarisation dips expected for the two level crossings at B_a and B_b, estimated for $\Delta M = 1$ only from the contributions of the different spin states of the muon to the two states at the field value of the crossing and hence independent of the mechanism responsible for the anticrossing. These ratios explain why the first crossing is difficult to detect in the LF-time integral mode experiment where the background repolarisation at low fields is prominent. However this crossing is clearly seen as a relaxation peak in the LF-time differential experiment (see Figure 9), due to the contribution of molecular dynamics to the mechanism of the ALC signal.

Finally it is possible to define a temperature of 584 K characteristic of ferrocene, as a μSR measure of the extent of spin-orbit interaction that is present in the Mu–metal adduct. Future experiments with other metallocenes will help to illucidate this aspect of the work.

Experimental Section

A sample of ferrocene purchased from Avocado Research Chemicals and further purified by sublimation was used for most of the experiments. A polycrystalline sample densely packed into a 2 mm deep and 40 mm diameter recess in an aluminium plate and covered with a thin mylar film was used for the muon spin relaxation experiments. These experiments were carried out using the EMU spectrometer at the ISIS muon facility, Rutherford Appleton Laboratory (RAL), UK. A similar sample arrangement, but with a backing plate of pure copper, was used for the time differential and time integral experiments at higher magnetic fields at the Paul Scherrer Institut (PSI), Switzerland. The spectrum of pure copper was used as a background (A slowly changing signal due to the effect of the change in magnetic field on the paths taken by the positrons from sample to detector.) for spectral subtraction in the ALC experiments.

Details of the μSR spectroscopic techniques are given in reference [1]. The dominant magnetic interaction in the case of muonium or of a muoniated radical was that between the muon and the radical electron. The evolution of the energy levels of such a hyperfine interaction was given by the well known Breit–Rabi diagram. An example of such a diagram with splitting of the triplet state due to spin-orbit coupling is shown in Figure 12. Longitudinal field muon spin relaxation in a four level system was treated by Cox and Sivia,[23] where they show that the muon relaxation function in the case of one radical species was in practice indistinguishable from a single exponential, allowing an effective relaxation rate $\lambda = T_1^{-1}$ to be extracted from a simulation.

Descriptions of the ALC technique are given by Roduner in several publications.[1] The energy levels shown in Figure 12 may not strictly cross if the following three conditions are satisfied. i) There should be an element in the Hamiltonian that leads to a mixing of the two states; ii) its magnitude should be large enough to cause an oscillation with a frequency ν_r, such that the time $\nu_r^{-1} h/\Delta E$ is comparable to or shorter than the muon lifetime; and iii) one of the eigenstates must belong to muon spin α, the other one to muon spin β. Two types of avoided crossings are possible depending on either the off diagonal element in the energy matrix mixing the two states directly or indirectly via coupling of both states to a common, energetically remote state. The signals thus observed are called avoided level crossing resonances (ALC), and sometime these are also referred to as anticrossing resonances or simply as level crossing resonances. There are three selection rules for the observation of ALC resonances where the total spin quantum number, M, can either change by 0, 1 or 2 units. $|\Delta M| = 1$ corresponds to a transition where only the muon spin flips. $|\Delta M| = 0$ corresponds to the situation where another spin $^1/_2$ nucleus such as that of a hydrogen atom in also involved. The latter would then be a muon–proton spin flip–flop transition. $|\Delta M| = 2$ gives a very much weaker and sharper signal, and it is due to a transition consisting of muon–proton spin flip–flip. The latter transitions are not often observed. Conventionally, these avoided level crossings are observed by monitoring the muon polarisation as a function of the applied longitudinal magnetic field, when any mixing gives rise to a polarisation loss. The field positions and band shapes of these polarisation dips may be used to evaluate the properties of the muoniated radical that is studied. The

spectra reported in this study are of polycrystalline samples, and these therefore give powder averaged spectra that in general show broad features.

Acknowledgements

We are grateful to Professor Manfred Bochmann, Dr. Carlo Kaiser, Dr. Rod Macrae and Dr. Paul Gubbens for useful discussions. The Paul Scherrer Institute, Villigen (Switzerland) and the ISIS facility, Rutherford Appleton Laboratory (UK) are thanked for beam-time and the associated facilities. The EPSRC is thanked for funding this work.

[1] D. C. Walker, *Muon and Muonium Chemistry*, Cambridge University Press, **1983**; E. Roduner, *Lecture Notes in Chemistry, Vol. 49*, Springer, Heidelberg **1988**; E. Roduner, *Chem. Soc. Rev.* **1993**, *22*, 337; *Muon Science. Muons in Physics, Chemistry and Materials*, Proceedings of the 51st Scottish Universities Summer School in Physics (Eds.: S. L. Lee, S. H. Kilcoyne, R. Cywinski), **1998**; for journal special issues on this topic see; *Appl. Magn. Reson.* **1997**, *13*; *Magn. Reson. Chem.* **2000**, *38*.

[2] K. Richardson, *Chem. Br.* **1994**, *30*, 87; A. D. Horton, *Trends Polym. Sci.* **1994**, *2*, 158; A. M. Thayer, *Chem. Eng. News* **1995**, *73*, 20.

[3] R. M. Waymouth, G. W. Coates, *Science* **1995**, *267*, 222.

[4] G. M. Wilmer, M. B. France, S. R. Lynch, R. M. Waymouth, *Organometallics* **2004**, *23*, 2405.

[5] I. D. Reid, T. Azuma, E. Roduner, *Nature* **1990**, *345*, 328.

[6] C. T. Kaiser, P. C. M. Gubbens, E. Kemner, A. R. Overweg, U. A. Jayasooriya, S. P. Cottrell, *Chem. Phys. Lett.* **2003**, *381*, 292.

[7] See for example: H.-H. Brintzinger, D. Fischer, R. Mülhaupt, B. Rieger, R. Waymouth, *Angew. Chem.* **1995**, *107*, 1255; *Angew. Chem. Int. Ed. Engl.* **1995**, *34*, 1143.

[8] See for example: M. L. McKee, *J. Am. Chem. Soc.* **1993**, *115*, 2818; M. J. Mayor-Lopez, J. Weber, B. Mannfors, A. F. Cunningham, Jr., *Organometallics* **1998**, *17*, 4983; M. J. Mayor-Lopez, H. P. Luthi, H. Koch, P. Y. Morgantini, J. J. Weber, *J. Chem. Phys.* **2000**, *113*, 8009.

[9] R. M. Macrae, *Phys. B* **2006**, *374–375*, 307.

[10] All experiments were based on muon implantation into samples of ferrocene in the solid state; no attempt was made to distinguish between radicals formed by muonium addition and those formed via muon addition followed by electron capture, since it does not affect the hyperfine spectroscopy of the end product. However, there is the possibility of significantly different formation mechanisms of Mu adducts at play at the two extremes of the temperature range 18 to 295 K thus giving rise to different initial muniated radical distributions.

[11] J. S. Griffith, *The theory of the Transition Metal Ions*, Cambridge University Press, Cambridge, **1971**.

[12] J. H. Ammeter, J. D. Swalen, *J. Chem. Phys.* **1972**, *57*, 678.

[13] E. O. Fischer, W. Z. Pfab, *Z. Naturforsch. B* **1952**, *7*, 377; P. F. Eland, R. J. Pepinsky, *J. Am. Chem. Soc.* **1952**, *74*, 4971; J. D. Dunitz, L. E. Orgel, *Nature* **1953**, *171*, 121.

[14] A. Kubo, R. Ikeda, D. J. Nakamura, *Chem. Soc. Faraday Trans. 2* **1986**, 1543.

[15] A. B. Gardner, J. Howard, T. C. Waddington, R. M. Richardson, J. Tomkinson, *Chem. Phys.* **1981**, *57*, 453.

[16] J. W. Edwards, G. L. Kingston, R. Mason, *Trans. Faraday Soc.* **1960**, *56*, 660.

[17] U. A. Jayasooriya, G. M. Aston, J. A. Stride, *Appl. Magn. Reson.* **1997**, *13*, 165.

[18] P. Seiler, J. D. Dunitz, *Acta. Crystallogr. B* **1979**, *35*, 1068.

[19] N. Fey, *J. Chem. Technol. Biotechnol.* **1999**, *74*, 852.

[20] J. C. Green, *Struct. Bonding* **1981**, *43*, 37.

[21] S. Evans, J. C. Green, S. E. Jackson, *J. Chem. Soc. Faraday Trans. 2* **1972**, 249.

[22] A. H. Cowley, *Prog. Inorg. Chem.* **1979**, *26*, 46.

[23] S, F. J. Cox, D. S. Sivia, *Hyperfine Interact.* **1994**, *87*, 971; S. F. J. Cox, D. S. Sivia, *Appl. Magn. Reson.* **1997**, *12*, 213.

[24] D. Yu, P. W. Percival, J. Borodovitch, S. Leung, R. F. Keifl, K. Venkateswaram, S. F. J. Cox, *Chem. Phys.* **1990**, *142*, 229; D. G. Fleming, D. J. Arseneau, J. Pan, M. Y. Shelley, M. Senba, P. W. Percival, *Appl. Magn. Reson.* **1997**, *13*, 181.

[25] K. Nakagawa, M. B. Candelaria, W. W. C. Chik, S. S. Eaton, G. R. Eaton, *J. Magn. Reson.* **1992**, *81*, 98.

[26] E. J. Ansaldo, J. Boyle, Ch. Niedermeyer, G. D. Morris, J. H. Brewer, C. E. Stronach, R. S. Carey, *Z. Phys. B* **1992**, *86*, 317; R. F. Kiefl, J. W. Schneider, A. MacFarlane, K. Chow, T. L. Duty, T. L. Estle, B. Hitti, R. L. Lichti, E. J. Ansaldo, C. Schwab, P. W. Percival, G. Wei, S. Wlodek, K. Kojima, W. J. Pomanow, J. P. McCauley, Jr., N. Coustel, J. E. Fischer, A. B. Smith III, *Phys. Rev. Lett.* **1992**, *68*, 1347; E. Roduner, P. W. Percival, P. Han, D. M. Bartels, *J. Chem. Phys.* **1995**, *102*, 5989.

[27] E. Kemner, I. M. de Schepper, G. J. Kearley, U. A. Jayasooriya, *J. Chem. Phys.* **2000**, *112*, 10926.

[28] M. B. Yim, D. E. Wood, *J. Am. Chem. Soc.* **1975**, *97*, 1004; D. G. Fleming, D. J. Arseneau, J. J. Pan, M. Y. Shelley, M. Senba, P. W. Percival, *Appl. Magn. Reson.* **1997**, *13*, 181.

[29] P. W. Percival, R. F. Kiefl, S. R. Kreitzman, D. M. Garner, S. F. J. Cox, G. M. Luke, J. H. Brewer, K. Nishiyama, K. Venkateswaran, *Chem. Phys. Lett.* **1987**, *133*, 465.

[30] E. Roduner, H. Fischer, *Chem. Phys.* **1981**, *54*, 261.

[31] D. G. Fleming, M. Y. Shelley, D. J. Arseneau, M. Senba, J. J. Pan, S. R. Kreitzman, E. Roduner, *Phys. B* **2000**, *289*, 603.

[32] C. T. Kaiser, P. C. M. Gubbens, E. Kemner, A. R. Overweg, U. A. Jayasooriya, S. P. Cottrell, *Chem. Phys. Lett.* **2003**, *381*, 292.

Received: June 18, 2006
Published online: December 13, 2006

